Spontaneous Substitutions on Phosphorus Trihalides in Imidazolium Halide Ionic Liquids: A Grotthuss Diffusion of Anions?

CHEMISTRY
A European Journal

A Journal of
ChemPubSoc Europe

Accepted Article

Title: Spontaneous Substitutions on Phosphorus Trihalides in Imidazolium Halide Ionic Liquids: A Grotthuss Diffusion of Anions?

Authors: Oldamur Holloczki, Alexander Wolff, Julia Pallmann, Rachel Whiteside, Jennifer Hartley, Matthias A. Grasser, Peter Nockemann, Eike Brunner, Thomas Doert, and Michael Ruck

To be cited as: *Chem. Eur. J.* 10.1002/chem.201803558

Link to VoR: http://dx.doi.org/10.1002/chem.201803558

Supported by
ACES

WILEY-VCH

10.1002/chem.201803558

Spontaneous Substitutions on Phosphorus Trihalides in Imidazolium Halide Ionic Liquids: A Grotthuss Diffusion of Anions?

Oldamur Hollóczki,[a,*] Alexander Wolff,[b] Julia Pallmann,[b] Rachel E. Whiteside,[c] Jennifer Hartley,[d] Matthias A. Grasser,[b] Peter Nockemann,[c] Eike Brunner,[b] Thomas Doert,[b] Michael Ruck,[b,e]

[a]Mulliken Center for Theoretical Chemistry, University of Bonn, Beringstr. 4+6, D-53115 Bonn, Germany

[b]Faculty of Chemistry and Food Chemistry, Technische Universität Dresden, D-01062 Dresden, Germany

[c]School of Chemistry and Chemical Engineering, Queen's University of Belfast, Belfast BT7 1NN, United Kingdom

[d]Institute of Inorganic Chemistry, TU Bergakademie Freiberg, D-09599 Freiberg, Germany

[e]Max Planck Institute for Chemical Physics of Solids, Nöthnitzer Str. 40, D-01187, Dresden, Germany

holloczki@gmail.com

August 29, 2018

10.1002/chem.201803558

TOC entry:

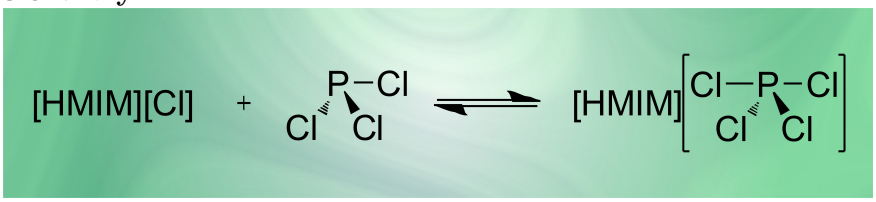

Phosphorus trihalides form $[PX_4]^-$ anions in 1,3-dialkylimidazolium halide ionic liquids. The dynamic exchange of the anions at the phosphorus atom shows typical characteristics of a Grotthuss-like diffusion mechanism, offering a potential way to design highly conducting materials.

10.1002/chem.201803558

PX_3 species (X = Cl, Br, I) in imidazolium halide ionic liquids combine with the anion Z (Z = Cl, Br, I) of the solvent, forming $[PX_3Z]^-$ complex anions. These anions are found to have a sawhorse shape, with the lone pair of the phosphorus atom filling the third equatorial position of the pseudo trigonal bipyramid. Theoretical results show that this association remains incomplete due to the strong hydrogen bonding with the ionic liquid cations, which competes with the phosphorus trihalide for the interactions with the Z^- anion. Temperature-dependent ^{31}P NMR experiments indicated that the P–Z binding is weaker at higher temperature. Both theory and experiments evidence a dynamic exchange of the halide anions at the phosphorus atom, together with continuous switching of the ligands at the phosphorus atom between equatorial and axial positions. The detailed knowledge on the mechanism of the spontaneous exchange of halogen atoms at phosphorus trihalides suggests a way to design novel, highly conducting ionic liquid mixtures.

1 Introduction

Phosphorus derivatives are manufactured and used around the globe in large quantities in a wide variety of fields. One of the most important precursors in the corresponding syntheses is phosphorus trichloride, which is produced annually in the several hundred thousand of tonnes range.[1] Among the many possible solvents, in which the synthesis of phosphorus compounds from e.g. PCl_3 can be performed, ionic liquids (ILs) have a remarkable potential. ILs are known as designer solvents,[2–5] which do not only provide a possible alternative to classical molecular liquids, but through their intricate network of intermolecular interactions[6–9] or their potentially high thermal stability[10–13] they also enable reactions that would be impossible in any other media.[2,5,14] Accordingly, significant scientific attention has been devoted to exploring the possibilities of combining the rich chemistry of phosphorus derivatives and the versatility of IL solvents.[15–19]

It was recently observed Ruck et al. that in 1-hexyl-3-methylimidazolium halide ionic liquids ([HMIm]Z; Z = Cl, Br, I) phosphorus trihalides (PX_3; X = Cl, Br, I), can readily undergo an X to Z halide exchange at the solute by the solvent,[20] offering an efficient way of interconverting these compounds into each other. The trends in the substitution showed a clear preference for the formation of the P–X bonds with the lighter halides, making PCl_3 the most persistent derivative in the investigated systems. Moreover, according to a strong, $\Delta\delta = 26$ ppm upfield shift of the ^{31}P NMR signal of PCl_3 in [HMIm]Cl, it was apparent that there is a specific and strong solute-solvent interplay in these systems, which may also play a role in the aforementioned substitution reactions. The nature of this interaction could be the coordination of the anion to the phosphorus similarly to metal chlorides such as $AlCl_3$ or $GaCl_3$,[21,22] but other interactions, such as hydrogen bonding,[6–8,23–25] or spontaneous carbene complex formation might also be possible.[26–29]

Such interactions between halide anions of IL-like materials and PCl_3 were also reported in a publication by Dillon et al.[30] In a co-crystal of tetraethylammonium chloride

and PCl_3, a short distance between the chloride anion and the phosphorus was observed by X-ray crystallography, whilst in acetonitrile an interaction between these atoms was indicated by Raman and ^{31}P NMR spectroscopy.[30] It is reasonable to assume that a similar coordination occurs also in the mixtures of PCl_3 and 1,3-dialkylimidazolium halide ILs, and that this process is involved in the reported[20] substitutions. However, a well-packed crystal or a solution in acetonitrile may behave very differently from an ionic liquid, while the triethylammonium cation studied by Dillon[30] is also very different from the in ILs most widely applied and strong hydrogen bond donor 1,3-dialkylimidazolium cation. These significant changes in the environment may influence greatly this delicate association, and thereby the aforementioned substitution[20] as well.

It is especially interesting to point out that analogous complex formation in the mixtures of halide ILs and the strong Lewis acid $AlCl_3$ or $GaCl_3$ allows for the formation of ionic liquids with varying Lewis acidity/basicity, which has been exploited in a number of catalytic applications.[22] Apart from the synthetic chemical benefit of a medium with tunable chemical character, some of the corresponding halogenoaluminate ILs have been shown to exhibit surprisingly high conductivities[31,32] due to a Grotthuss-like diffusion process of the halide anions in them.[33] Accordingly, it is also interesting to consider that the present IL-PCl_3 mixtures may have similar properties, and beyond the connected synthetic relevance they may also be employed in future electrochemical devices. Clearly, the Lewis acidity of PCl_3 is significantly different from that of $AlCl_3$, hence such IL-PCl_3 mixtures could be a useful element to the palette of IL mixtures with specific properties.

Thus, characterizing the interactions between phosphorus trihalides and 1,3-dialkylimidazolium halide ionic liquids at a molecular level would contribute greatly to the application of these ILs as reaction media for the reactions of phosphorus trihalides, while it would perhaps also open further possibilities in the broader field. For this reason, in this combined theoretical and experimental study the behavior of PX_3 derivatives in 1,3-dialkylimidazolium ionic liquids with chloride, bromide and iodide anions is explored;

to understand the mechanism of the substitution reactions, and to assess the possibility of designing novel, highly conducting electrolytes.

2 Experimental Methodologies

Starting Materials

For the NMR and Raman experiments, the ILs 1-hexyl-3-methylimidazolium chloride (IoLiTec, 99 %), 1-hexyl-3-methylimidazolium bromide (IoLiTec, 99 %) and 1-hexyl-3-methylimidazolium bis(trifluoromethylsulfonyl)imide (IoLiTec, 99 %) were dried at 110 °C for 12 h under vacuum. To remove even traces of water for the synchrotron experiments, the ILs were dried at 70 °C for 24 h, at 110 °C for 12 h and finally at 200 °C for 1 h under dynamic vacuum ($p < 0.1$ Pa). Phosphorus trichloride (Sigma-Aldrich, 99%) was used without further purification.

Sample Preparation

All compounds were handled in an argon-filled glovebox (M. Braun; $p_{O2}/p_0 < 1$ ppm, $p_{H2O}/p_0 < 1$ ppm). In a typical synthesis, 0.5 mmol of a phosphorus trichloride was added to 10.0 mmol of an IL in a small beaker. The mixture was stirred manually at room temperature for several minutes.

NMR Spectroscopy

The samples were transferred into tubes with gas-tight polytetrafluorethylene valves (Deutero) in a glovebox. Dimethyl sulfoxide-d6 contained inside a sealed capillary in the NMR tubes as external lock. The NMR experiments were performed using an AVANCE III HDX, 500 MHz Ascend spectrometer (Bruker). The ^{1}H and ^{31}P NMR spectra were recorded at resonance frequencies of 500.13 MHz and 202.45 MHz, respectively, by using a 5 mm high-resolution CryoProbe Prodigy probe head. The spectra were measured

using a 90° pulse and relaxation delays of 2 s (for both nuclei). The ^{1}H and ^{31}P chemical shifts were referenced externally to δ(Tetramethylsilane) = 0.0 ppm and $\delta(H_3PO_4$; 85 %) = 0.0 ppm, respectively.

Raman Spectroscopy

The samples were transferred into customized gas-tight 5 mm glass tubes in a glovebox. The Raman spectroscopy experiments were carried out using a RFS 100 (Bruker), equipped with a 1024 nm Nd-YAG Laser with a resolution of 4 cm^{-1}.

X-ray Absorption Spectroscopy

The samples were transferred into costume-made plastic cells and sealed with Ultralene® foil under glovebox conditions. The X-ray absorption spectroscopy (XAS) was performed at the BESSY II light source at the KMC-1 beamline (Helmholtz-Zentrum Berlin).[34] A four-bounce scanning Si(111) monochromator was used and the phosphorous K-edge was probed. The measurements were performed in fluorescence geometry with a XFlash 4010 detector (Bruker). The data from a single scan was used in this study. Multiple scans showed identical spectra, indicating that the sample was not degenerated under the impact of the beam. XANES spectra were normalized as a function of IT/I0.

3 Theoretical Methods

Static DFT and ab initio Calculations

All static density functional theory (DFT) calculations were performed by using the ORCA 3.0.3 program package.[35] In these calculations the B3LYP functional[36–38] was applied with the D3 dispersion correction with Becke–Johnson damping,[39,40] together with the def2-TZVPP basis set.[41] For both the SCF convergence and the geometry optimization tight settings of ORCA were applied. The eigenvalues of the Hessian were

calculated after all optimizations to verify the nature of the obtained stationary point. The analysis of the wavefunction was performed by the Multiwfn program,[42] except for the shared electron number[43] data, which was produced by using the ridft module[44,45] of the Turbomole V6.5 program[46] with the same methods and settings as described above.

Ab initio Molecular Dynamics Simulations

Due to the immense computational demand of ab initio molecular dynamics (AIMD) simulations, instead of the 1-hexyl-3-methylimidazolium halide [HMIm]Z ILs of the experiments, 1-butyl-3-methylimidazolium halide [BMIm]Z ILs were studied here by AIMD. With this slight simplification not only systems with more ion pairs were possible to simulate, which represents better models for the bulk liquids, but also longer simulations became accessible, which is advantageous to ensure a better sampling. All AIMD simulations were performed under periodic boundary conditions, using the Quickstep module of the CP2K program package.[47] The electronic structure was modeled with the BLYP functional[37,38,48] enhanced by the D3 dispersion correction with Becke–Johnson damping,[39,40] together with the MOLOPT-DZVP basis set[49] for the valence electrons. The core electrons were handled through Goedecker–Teter–Hutter pseudopotentials.[50–52] The settings of multigrid level 5 and a cutoff criterion of 400 Ry were chosen, with a convergence criterion for the SCF cycle of 10^{-5}. The timestep for the MD simulations was chosen to be 0.5 fs.

system	solute	solvent	cell vector / Å	ρ / g cm^{-3}
I	PCl_3	[BMIm]Cl	22.64	1.020
II	PCl_3	[BMIm]Br	23.03	1.210
III	PCl_3	[BMIm]I	23.53	1.371
IV	PBr_3	[BMIm]Cl	22.64	1.039
V	PI_3	[BMIm]Cl	22.64	1.059

Table 1: Physical parameters of the simulation boxes, and the length of the corresponding simulations.

The cubic simulation boxes of systems **I-III**, consisting of 40 ion pairs of the IL and a single molecule of PCl_3, were created by using the Packmol program[53] to represent the density of the pure IL. Systems **IV** and **V** were created by replacing the PCl_3 molecule in system **I** by the corresponding phosphorus halide. The resulting cell parameters and densities are collected in Table 1. First, the cell was optimized with the default settings of the CG optimizer to avoid possible energy hotspots. A 7.5 ps equilibration run was performed in an NVT ensemble, applying a massive Nosé–Hoover thermostat at a higher temperature (T = 500.00 K, τ = 100 fs) with an individual thermostat for each atoms to ensure the activation of all degrees of freedom. The subsequent production run was performed at 298.15 K, with a global thermostat for the whole system. The analysis of the results was performed with the TRAVIS program.[54]

4 Results and Discussion

To explore the nature of the interaction between the ionic liquid solvent and the phosphorus trihalide, we first performed a series of experiments on the PCl_3/[HMIm]Cl system, which exhibited the largest ^{31}P NMR shift in our previous study.[20] Through XAS measurements of these mixtures it was confirmed that the oxidation state of the phosphorus is not changed upon dissolving in this IL (Figure S1 in the Supp. Inf.). If any structure-influencing hydrogen bonding with the imidazolium cation should be involved in the solute-solvent interactions, or if a carbene — formed from the IL cation[26–28] — should coordinate the phosphorus atom, the ^{1}H NMR spectrum of the liquid should exhibit specific differences in the presence of the phosphorus compound. However, the ^{1}H NMR spectra of [HMIm]Cl are very similar in the presence and absence of PCl_3 (Figure 1), with no extra peaks when the phosphorus derivative is added to the solution. This finding excludes the formation of carbene complexes, and any major changes in the hydrogen bonding environment of the cation.

In the light of the earlier results with analogous systems,[30] and due to the lack of

10.1002/chem.201803558

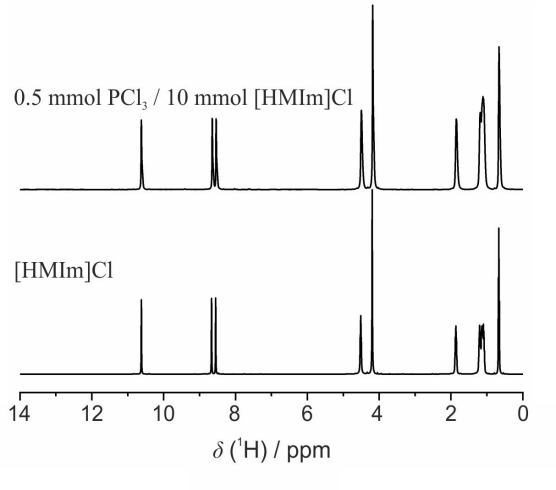

Figure 1: ^{1}H NMR spectra of the neat [HMIm]Cl (below), and its mixture with PCl_3 (above) at room temperature.

significant interactions with the cation, we focused on the anion-PCl_3 interplay. By using ^{31}P NMR spectroscopy, we could reproduce the previously reported[20] large shift in the signal of the PCl_3 in [HMIm]Cl (Figure 2), which matches the findings of Dillon et al. as well.[30] However, the ^{31}P signal of PCl_3 in the neat liquid and in [HMIm][NTf_2] with the non-coordinating bis(trifluoromethylsulfonyl)imide NTf_2 anion, were found at the same position ($\Delta\delta \approx 0.6$ ppm, Figure 2), in agreement with earlier reports.[18,19] These findings clearly show that the interplay between the [HMIm]Cl and the PCl_3 is largely the interaction between the chloride and the phosphorus atom.

The Raman spectra for the neat PCl_3 showed the symmetric (ν_1, A_1) and asymmetric (ν_3, E) stretching vibrations, as well as the symmetric (ν_2, A_1) and asymmetric (ν_4, E) bending modes at 513, 487, 260 and 190 cm^{-1}, respectively, are in good agreement with literature (Figure S2 in the Supp. Inf.).[55] For the PCl_3 dissolved in [HMIm][NTf_2] the bands were found at almost identical positions (Figure S3 in the Supp. Inf.). For PCl_3 in [HMIm]Cl, however, a shift in the symmetric stretching vibration by -18 cm^{-1}, and the symmetric bending mode by -6 cm^{-1} was observed (Figure S4 in the Supp. Inf.). The shift in these bands is consistent with the elongation of a P–Cl bond in [PCl_4]$^{-}$,

10.1002/chem.201803558

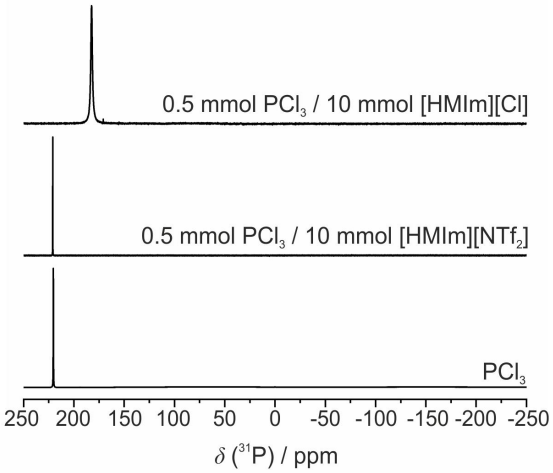

Figure 2: ^{31}P NMR spectra of the pure PCl_3 (below), PCl_3 in the non-coordinating [HMIm][NTf_2] (middle), and PCl_3 in the [HMIm]Cl (above) at room temperature.

which induces a decrease in the bond strength, shifting the vibrations toward smaller wavenumbers.

The nature of the chloride-PCl_3 interaction in the IL is likely to be an association, similar to that observed for this phosphorus compound in tetraethylammonium chloride.[30] This reaction was shown to be an equilibrium between $[PCl_4]^-$ and PCl_3, based on the dependence of the ^{31}P NMR shifts on the chloride concentration.[30] Similarly to the concentrations, the temperature can also show a strong effect on the equilibrium, with exothermic reactions suppressed at higher temperatures. Thus, to further prove the formation of $[PCl_4]^-$ anions in the solution, the ^{31}P NMR spectra of PCl_3 in [HMIm]Cl was measured also at various temperatures. While pure PCl_3 and PCl_3 in [HMIm][NTf_2] both showed almost identical and only slight changes ($\Delta\delta/\Delta T = 0.015$ ppm/K) in the position of the signal, in [HMIm]Cl a large, downfield shift of $\Delta\delta/\Delta T = 0.132$ ppm/K was observed (Figure 3). In other words, by increasing the temperature, the PCl_3 in the chloride-containing IL became more and more similar to neat PCl_3. This is consistent with an equilibrium of $PCl_3 + Cl^- \rightleftharpoons [PCl_4]^-$, which is slightly exothermic toward the

10.1002/chem.201803558

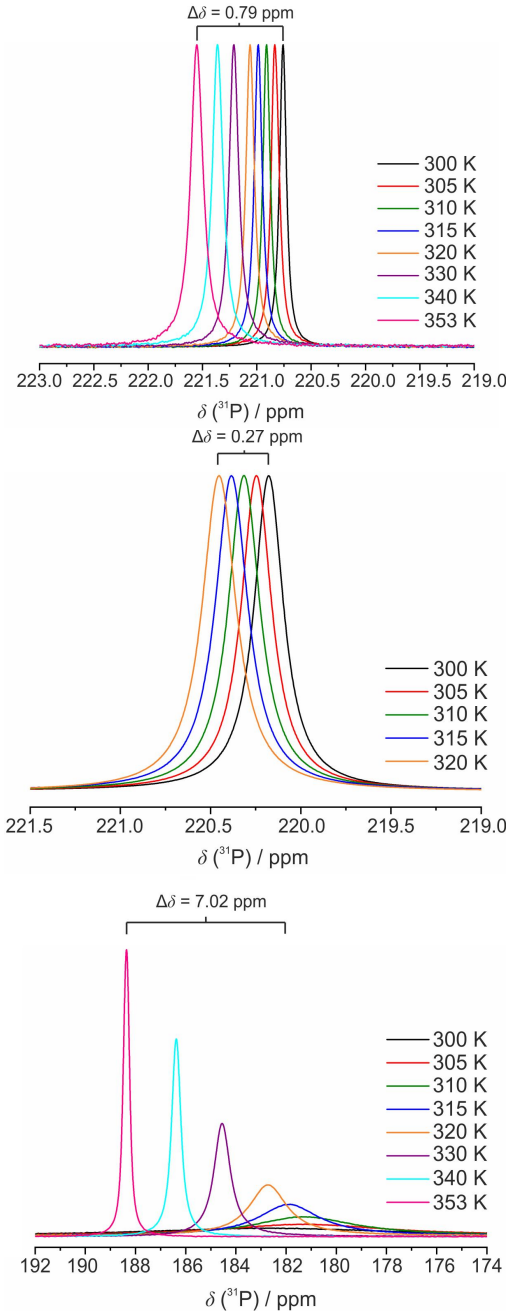

Figure 3: Temperature dependence of the ^{31}P NMR spectra of the pure PCl_3 (above), PCl_3 in the non-coordinating [HMIm][NTf_2] (middle), and PCl_3 in the [HMIm]Cl (below).

10.1002/chem.201803558

association, and is, therefore, shifted to the left side by the increase of temperature.

Thus, the experiments above gave a clear indication that the chloride anion from [HMIm]Cl interacts strongly with PCl_3, which appears to be an association of these two species to form $[PCl_4]^-$. To investigate the structure of this anion, a series of static quantum chemical calculations were performed. The geometry of $[PCl_4]^-$ optimized in the gas phase exhibits a sawhorse-shaped pseudo trigonal bipyramidal geometry (Figure 4), which is in agreement with the previous X-ray crystallographic data on similar systems.[30] However, unlike in the previous experiments, in these calculations a C_{2v} symmetry was observed for $[PCl_4]^-$, with the two equivalent axial P–Cl bonds (Table 2). It is clear from all the bond indices for the P–Cl bonds listed in Table 2 that upon coordination of the chloride anion to the phosphorus, the individual P–Cl bonds become longer and weaker compared to the parent trichloride. Under closer scrunity, the equatorial P–Cl bonds are only slightly longer than those in PCl_3, and significantly shorter than the axial bonds. The molecular orbitals demonstrate that the structure of $[PCl_4]^-$ is possible to characterize through a three center four electron bond that includes the two axial chlorine atoms (S5 in Supp. Inf.).[56]

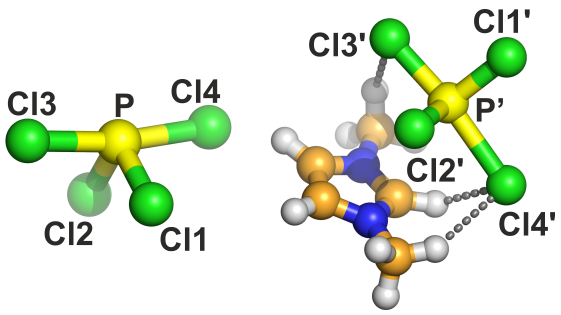

Figure 4: Structure of the $[PCl_4]^-$ complex and the [MeMIm][PCl_4] ion pair (C: orange; N: blue; Cl: green; P: yellow; H: white).

This gas phase geometry is, however, idealized, obtained in the complete lack of temperature and solvent effects. This is visible also in the calculated ^{31}P NMR signals: For the isolated $[PCl_4]^-$ a $\Delta\delta = 65$ ppm upfield shift was calculated compared to PCl_3,

overestimating by far the experimentally found $\Delta\delta = 26$ ppm at room temperature. To identify the effects that induce the difference between the experimentally[30] found structure and the geometry optimized in the gas phase, we repeated the geometry optimizations of the $[PCl_4]^-$ in the presence of an 1,3-dimethylimidazolium ($[MMIm]^+$) cation.

Indeed, the structure of this complex anion changes significantly by including the counterion (Figure 4 and Table 2). In the corresponding ion pair one of the P–Cl bonds is elongated and weakened, breaking the symmetry of the free $[PCl_4]^-$ by a partial departure of a chloride anion. The rest of the P–Cl bonds becomes shorter and stronger compared to those in the free $[PCl_4]^-$, while through the decrease in the charge delocalization a stronger hydrogen bond can be formed between the departing chloride and the cation; all compensating for the energy loss of the partial breaking of a P–Cl bond. In other words, these findings suggest that the elongation of one of the axial P–Cl bonds in the crystal structure,[30] and presumably also in the liquid, is due to the delicate balance between inter- and intramolecular interactions, along with the coordination of the chloride anion to the phosphorus, which is partly suppressed by the chloride-cation interplay. This also explains why no significant changes in the ^{1}H NMR spectra were observed when dissolving PCl_3 in the IL. Due to the limited strength of the Cl^--PCl_3 interplay, the hydrogen bonding ability of the associated chloride anion is barely altered, interacting with the cation with a similar strength. Considering the temperature dependence of the ^{31}P NMR signal (Figure 3), the increasing shift at lower temperature corresponds to more $[PCl_4]^-$. In agreement, the experimental values resemble more the calculated $\Delta\delta = 65$ ppm when extrapolating the measured data to 0 K ($\Delta\delta = 92$ ppm, Figure S6 in the Supp. Info.).

According to these calculations, solvent and temperature effects should have a significant influence on the formation and structure of $[PX_3Z]^-$ species. Thus, to understand the formation of these anions, a full model of the bulk liquid has to be considered, to-

bond	position	length /Å	Mayer BI	Mulliken BI	Wiberg BI	SEN
PCl_3	-	2.070	1.15	0.51	0.94	1.71
P–Cl1	equatorial	2.107	1.05	0.42	0.91	1.58
P–Cl2	equatorial	2.107	1.05	0.42	0.91	1.58
P–Cl3	axial	2.410	0.67	0.18	0.39	1.06
P–Cl4	axial	2.410	0.67	0.18	0.39	1.06
P′-Cl1′	equatorial	2.057	1.15	0.54	0.99	1.72
P′-Cl2′	equatorial	2.100	1.06	0.45	0.91	1.58
P′-Cl3′	axial	2.275	0.81	0.25	0.56	1.27
P′-Cl4′	axial	2.620	0.45	0.10	0.21	0.71

Table 2: Electronic structure and bonding parameters (BI: Bond Index; SEN: Shared Electron Number) in PCl_3 (top), in an isolated $[PCl_4]^-$ in the gas phase (middle), and in a [MeMIm][PCl_4] ion pair (bottom) for each P–Cl bond. A picture of the structures and the labeling can be seen in Figure. 4

gether with the underlying dynamic effects. For this reason we performed a set of ab initio molecular dynamics (AIMD) simulations on PX_3 in [BMIm]Z (see Table 1), in which these effects can be directly tracked, while the explicit treatment of the electronic structure also allows reactions to occur.

In all simulations, the phosphorus atom became tetracoordinated already during the equilibration phase through the $PX_3 + Z^- \rightleftharpoons [PX_3Z]^-$ process. The forming structures exhibit the sawhorse-shaped structure (Figure 5), which was seen in the static quantum chemical calculations above, and the earlier[30] experimental reports. The bonding in the $[PX_3Z]^-$ structures can be discussed most straightforward for system **I**, where all X and Z halogen atoms are of the same kind, and therefore the bond lengths can be directly used to compare the strength of the individual interactions (Figure 6). According to the bond distances, altogether three kinds of P–Cl bonds can be distinguished, similarly to that observed for the [MMIm][PCl_4] ion pair in the static DFT calculations. The two equatorial P–Cl bonds are the shortest at 2.1-2.2 Å, followed by an axial chlorine at a distance of 2.3-2.4 Å, and finally a somewhat even more loosely coordinated anion at the distance of 2.5-2.8 Å, in an elongated axial position. The bond lengths observed in crystallographic experiments for an analogous system[30] are within the same range.

10.1002/chem.201803558

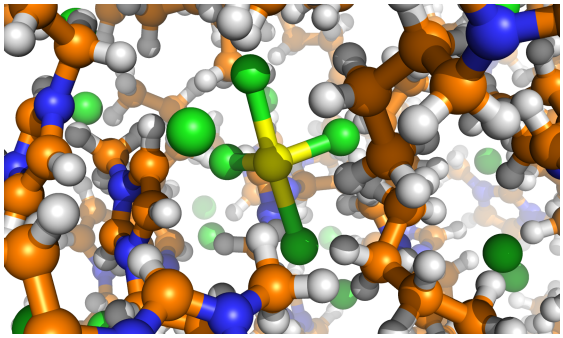

Figure 5: PCl_3 in [BMIm]Cl forms $[PCl_4]^-$, as shown from the present snapshot (C: orange; N: blue; Cl: green; P: yellow; H: white).

Interestingly, a dynamic change in the structure can be observed throughout the simulation. In the development of the relevant P–Cl distances in system **I** between 14 and 19 ps and between 28 and 34 ps of the simulation the most loosely coordinating axial chloride atom departs from the complex anion (brown and blue curves in Figure 6), resulting in the decrease in all the other P–Cl distances, respectively. During these two time intervals the three P–Cl bonds are apparently equivalent (black, red, and green curves in Figure 6), showing that momentarily the PCl_3 molecule is present in the liquid and not $[PCl_4]^-$. The leave of the most weakly coordinated chloride anion allows the coordination of another chloride anion from the bulk of the liquid, approaching the phosphorus atom shortly after the formation of the free PCl_3 molecule. Thus, the exchange of the coordinating halide anions in $[PCl_4]^-$ evidently occurs through a dissociative path, where the breaking of the P–Cl bond precedes the formation of the new one, similarly to an S_N1 reaction. This mechanism is in accordance with the Coulombic repulsion between the leaving and approaching anions.

The exchange between the chloride atoms at different positions within the $[PCl_4]^-$ anion can also be observed. The axial P–Cl bond can be increased in length, while the longer and weaker axial coordination at the opposite side of the phosphorus can be simultaneously shortened, see orange and black curves at 44 ps in Figure 6. Similarly, the

10.1002/chem.201803558

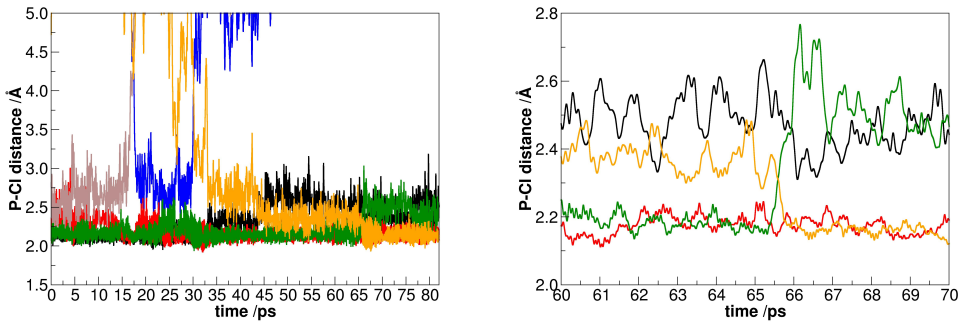

Figure 6: Development of relevant P–Cl distances in system **I** through the simulation. Each P–Cl distance is respresented by a different color. On the right the 60-70 ps interval is magnified to track a major conformational change within $[PCl_4]^-$.

axial and equatorial position chlorine atoms can undergo an exchange. This relatively fast process occurs for example between 65 and 66 ps in Figure 6, where an equatorial P–Cl bond (green) becomes a loosely coordinated axial bond, the axial P–Cl bond (orange) becomes equatorial, while the longest bond (black) is shortened to be the more covalent axial P–Cl bond. In this conformational change the lone pair and one chlorine retain their equatorial position, and therefore its mechanism cannot be described as a classical Berry pseudorotation,[57] where two axial and two equatorial ligands change their location within a trigonal bipyramidal structure.

The dynamic process of the anion coordination and departure at the phosphorus atom is highly similar to the Grotthuss-like diffusion process in chloroaluminate ionic liquids,[33] which has been shown to result in an order of magnitude higher conductivity for these materials than for other ILs.[31,32] The attachment of one halide, to form an axial P–Cl bond on one end of the molecule, allows the other axial P–Cl bond to break, delivering a chloride anion farther in space from the position of the first one, facilitating, therefore, the conduction process in these materials. For the efficiency of this process, however, both ends of this accepting-then-delivering mechanism should be tuned, which will be an interesting topic of interest in the future in the application of these systems.

X	Z	ΔE_{assoc}	ΔE_{subst}
Cl	Cl	−29.3	0.0
Cl	Br	−21.6	12.4
Cl	I	−16.0	21.4
Br	Cl	−38.5	−12.1
Br	Br	−26.8	0.0
Br	I	−20.9	8.5
I	Cl	−43.6	−19.7
I	Br	−32.9	−8.0
I	I	−25.6	0.0

Table 3: Reaction energies of the reactions $PX_3 + Z^- \rightleftharpoons [PX_3Z]^-$ (ΔE_{assoc}) and $PX_3 + Z^- \rightleftharpoons PX_2Z + Z^-$ (ΔE_{subst}) at the B3LYP-D3BJ/def2-TZVPP level of theory in kcal mol^{-1} units.

As we have shown above, the exchange of the halogen atoms at the phosphorus and those of the solvent occurs in the simulations. From the chemical point of view those cases are the most interesting, in which these halogen atoms are different, so the substitution results in another phosphorus compound. The quantum chemically calculated $PX_3 + Z^- \rightleftharpoons [PX_3Z]^-$ reaction energies (ΔE_{assoc}), thus the energetics of the association for the different phosphorus trihalides PX_3 and different halide anions Z^- in the gas phase are collected in Table 3. The data therein shows that the coordination strengths decrease in the order of $Cl^- > Br^- > I^-$ for the Z^-, and in the $PI_3 > PBr_3 > PCl_3$ order for the phosphorus derivatives. In other words, the heavier phosphorus trihalides are the more prone to react with the anions, and the lighter halide anions coordinate more strongly to the phosphorus. This is in accordance with the corresponding heats of formation for PX_3 compounds.[58] Since the attachment of the lighter halide anions to the PX_3 molecule is energetically more favorable than that of the heavier halides, and the abstraction of the heavier halides is energetically less demanding than that of the lighter ones, these trends result in the facile exchange of heavier halogen atoms to lighter ones at the phosphorus center, as observed earlier.[20] Indeed, the ΔE_{subst} energy of the substitution reaction $PX_3 + Z^- \rightleftharpoons PX_2Z + X^-$ shows a trend that is in line with this reasoning.

Turning to the liquid models, in systems **II** and **III** a PCl_3 molecule is dissolved in a

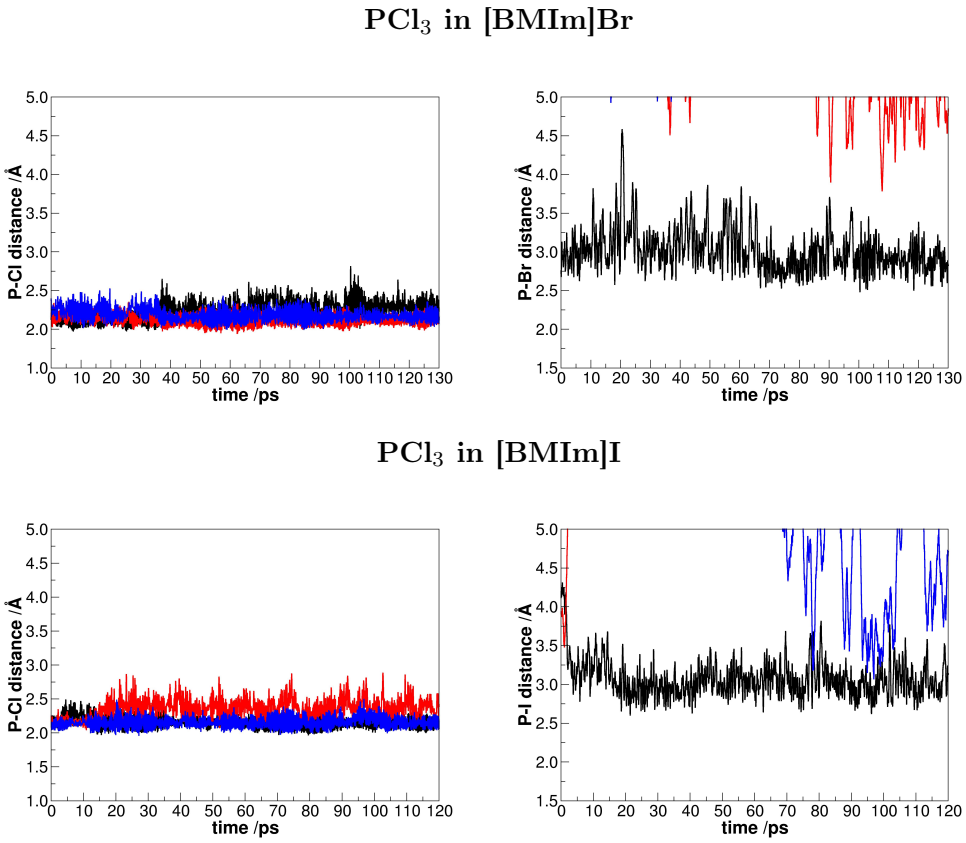

Figure 7: Development of the P–Cl distances (above left) and relevant P–Br distances (above right) in system **II**, and that of the P–Cl distances (below left) and relevant P–I distances (below right) in system **III** through the simulations. Each P–X and P–Z distance is respresented by a different color.

[BMIm]Br and [BMIm]I solvent, respectively. Similarly to system **I**, in these mixtures the coordination of a halide anion from the solvent to the phosphorus atom was observed during the 7.5 ps long equilibration (Figure 7 top right and bottom right). In both cases, the P–Cl bonds remain unbroken throughout the simulation, and in each system only one of them is elongated notably to ca. 2.4 Å, which resembles the more strongly bound of the two axially positioned P–Cl bonds in system **I**. The rest of the P–Cl bonds assume an equatorial position with shorter bond lengths. Exchange can be observed in between these two kinds of P–Cl bonds in the systems, see e.g. blue and black curves

at 35 ps in system **III** (Figure 7 bottom left), but the covalent bond between P and Cl is not broken in the simulations. According to these results, it is clear that the P–Br and P–I interactions are the weakest in these solutions, due to the apparently dominating strength of the P–Cl bonds. This is in good qualitative agreement with the static quantum chemical calculations above (Table 3), and previous results, suggesting that PCl_3 is stable in [HMIm]Br and [HMIm]I, and does not undergo a substitution reaction.[20]

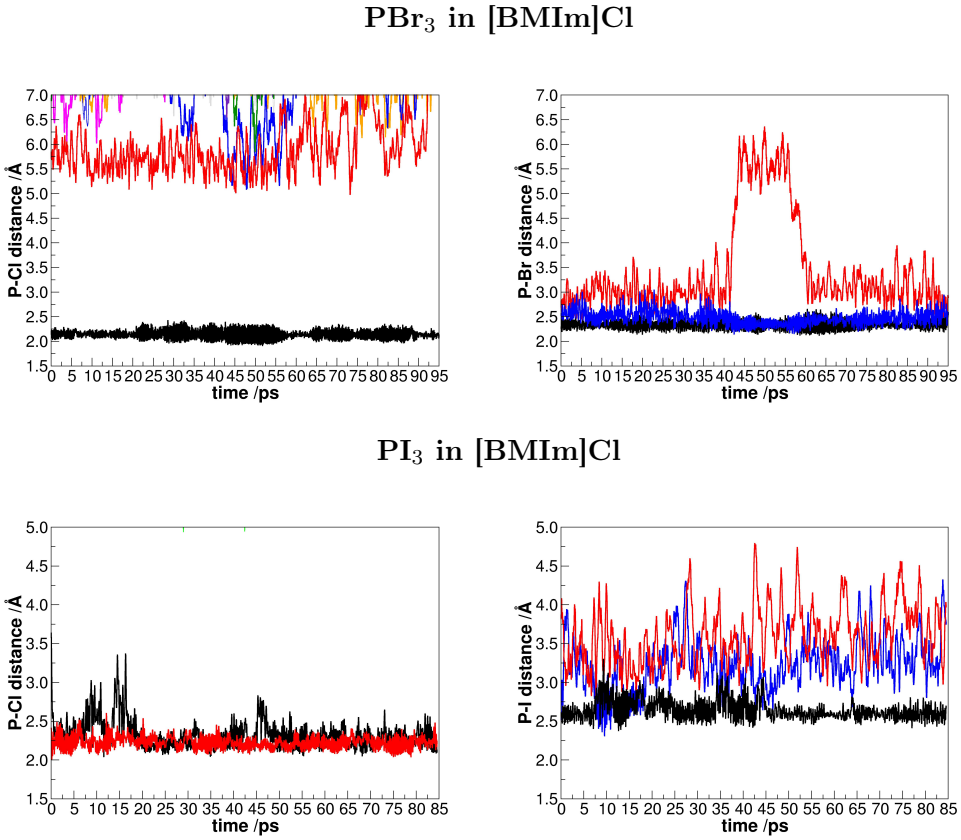

Figure 8: Development of the relevant P–Cl distances (above left) and all P–Br distances (above right) in system **IV**, and that of the relevant P–Cl distances (below left) and all P–I distances (below right) in system **V** through the simulations. Each P–X and P–Z distance is respresented by a different color.

In case of systems **IV** and **V** PBr_3 and PI_3 was dissolved in the [BMIm]Cl solvent,

respectively. In these simulations the chloride anion of the IL was again found prone to form a P–Cl bond. The corresponding interactions occurred as early as the equilibration in both cases. In case of the PBr_3, a single chloride anion coordinated to the phosphorus derivative, with a P–Cl distance of 2.1-2.2 Å (Figure 8 top left), which shows a good agreement with the equatorially positioned P–Cl bond in system **I**. The bromine atoms, on the other hand, are situated at three separate distance intervals within $[PBr_3Cl]^-$ during the simulation (Figure 8 top right), which shows that the equatorial, stronger axial and weaker axial positions are all occupied by these atoms. Moreover, one of the bromines departs the phosphorus at 42 ps, and stays in the solution about 5.8 Å away from the phosphorus atom as an isolated bromide anion for a ca. 20 ps period (red line in Figure 8 top right), leaving behind a PBr_2Cl molecule, which is visible also at the identical P–Br bond lengths for the other two bromine atoms during this time interval.

In case of system **V**, two iodine atoms are replaced by two chlorine atoms during the equilibration. This result clearly indicates that PI_3 is very prone for substitution in these environments. In this case, however, the two chlorine atoms that are bound to the phosphorus atom are most often both situated at similar, short distances. The three iodine atoms, on the other hand, show rather different bonding situation. Apparently, one of the iodine atoms is bound to the phosphorus throughout the whole simulation (black line in Figure 8 bottom right). The other two iodine atoms are, however, situated at a rather large distance (mostly above 3.0-3.5 Å), showing movements in a large radial distance interval. Thus, the molecule in the solution here is a rather free PCl_2I. The occasional close approach of the iodide anions to the phosphorus to form $[PCl_2I_2]^-$ affects the bonding in the molecule greatly: It is visible that at ca. 8, 16, 36, 45 and 64 ps the shorter P–I distances (blue curve in Figure 8 bottom right) result in the simultaneous increase in the other P–I bond length (black curve in Figure 8 bottom right), and in one of the P–Cl bond lengths as well (black curve in Figure 8 bottom left). Thus, in effect, a spontaneous substitution reaction was observed in the simulations of the systems **IV**

and **V**, which is in accordance with earlier experimental findings.[20] It is reasonable to assume that the fact that one (in case of PI_3) or two (in case of PBr_3) halogen atoms were not substituted spontaneously in these computer experiments by the anions of the solvent are simply due to the limitation of the present calculations in terms of simulation time. In fact, the diffusion of the departed halide anions from the proximity of the solute to the bulk of the solvent is beyond the reach of ab initio molecular dynamics in the present liquids with such slow dynamics.

From the point of view of the aforementioned potential applications based on the Grotthuss diffusion in these systems, the data in Table 3 can provide a good starting point. Clearly, if applying these systems for their conductivities, the halide on the phosphorus and in the IL should be the same, to avoid undesired substitution reactions, and to allow the release of another anion from the complex anion than the one that initially coordinated to the phosphorus. By varying the anion, the molar ratio of the PX_3 in the IL, and the temperature, the conductivity must show significant changes. The nature of the halide affects the viscosity of the IL, the mobility of the ions,[59,60] and the orientation of the ions within the liquid,[61,62] hence even if ΔE_{assoc} is similar for all three PX_3/[BMIm]Z ($X = Z$) systems considered here, the diffusivity must be different. Accordingly, among the three possible halides it is difficult to decide at this point which one could be an ideal candidate for designing highly conductive materials.

5 Summary and Conclusions

In this combined theoretical and experimental study we demonstrated that phosphorus trihalides in 1,3-dialkylimidazolium halide ionic liquids undergo a association with the anion of the solvent. The isolated $[PCl_4]^-$ has a C_{2v} symmetry and the shape of a sawhorse. Including the lone pair in equatorial position, a trigonal bipyramid results. In the presence of cations this symmetric structure is distorted, and one of the axially positioned P–Cl bonds is elongated. This can be explained by the formation of hydrogen

bonds between the cation and the departing chloride, which is stronger than it would be with $[PCl_4]^-$, where the negative charge is largely delocalized.

Molecular dynamics simulations for multiple combination of different phosphorus halides and 1-butyl-3-methylimidazolium halides, as well as NMR experiments for PCl_3 and 1-hexyl-3-methylimidazolium chloride showed that this association is a dynamic equilibrium between the free PX_3 molecule and the $[PX_3Z]^-$. While in the ab initio molecular dynamics simulations the P–Z bond formation and cleavage processes could be observed along the trajectories, in the ^{31}P NMR experiments a strong temperature dependence of the phosphorus chemical shift was observed, indicating less $[PX_3Z]^-$ at higher temperature. Similarly, the chlorine atoms at a phosphorus also often rearranged in the simulations, showing that the exchange of halides between the complex anion and the liquid is possible, in agreement with the experimental findings that such substitution reactions occur spontaneously. Apparently, the heavier phosphorus trihalides have a higher affinity than lighter ones to host a halide anion in a $[PX_3Z]^-$ anion, and the coordination of a lighter halide anion is more prone than heavier ones to bind to any given phosphorus trihalide. These trends result in the experimentally found preference[20] of heavier phosphorus halide to exchange their halogen atom to lighter ones in these systems.

In the light of these results the chemistry of phosphorus in these ionic liquids has a notable potential. The formation of these structures, and the connected spontaneous substitution reactions may allow reactions for the synthesis of phosphorus derivatives that would not be possible otherwise. Moreover, the consequences of the present findings reach farther than the mere synthetic advantages. The observed dynamic binding and release of anions to and from phosphorus trihalides in these systems have all the characteristics of a potentially highly conducting system, where the ionic conductivity stems mainly from a Grotthuss-like diffusion of the halide anions. This attractive feature makes these mixtures similar to e.g. halogenoaluminate ionic liquids, offering possible novel materials to the palette of electrolytes that can be produced for a lower price (PCl_3 is currently

about four times cheaper than $AlCl_3$). The underlying processes will be investigated in the close future in our group.

6 Acknowledgement

We would like to thank the Helmholtz Zentrum Berlin (HZB) for beamtime grants (proposal no. 16204691ST and 17205848ST) and for the respective travel funding. We gratefully acknowledge Dr. Dirk Wallacher (HZB) for developing the XANES measurement cells and for the excellent technical support as well as Dr. Roberto Felix Duarte (HZB) for supervision at the KMC-1 station. Maximilian Knies (TU Dresden) and Tobias Pietsch (TU Dresden) are also thankfully acknowledged for experimental support at the beamline. We would also like to thank Prof. Dr. Jan J. Weigand (TU Dresden) for providing us NMR facilities. Finally, we thank the Deutsche Forschungsgemeinschaft for financial support within the Priority Program SPP1708.

7 Supporting Information

Supporting Information containing the XAS, and Raman spectra, temperature dependent ^{31}P NMR data, as well as a figure with the relevant molecular orbitals of $[PCl_4]^-$ is available.

References

[1] Greenwood, N. N.; Earnshaw, A. *Chemistry of the Elements;* Elsevier: 2012.

[2] Welton, T. *Chem. Rev.* **1999,** *99,* 2071-2084.

[3] Welton, T. *Green Chem.* **2011,** *13,* 225.

[4] Rogers, R. D.; Seddon, K. R. *Science* **2003,** *302,* 792–793.

[5] Hallett, J. P.; Welton, T. *Chem. Rev.* **2011,** *111,* 3508–3576.

[6] Zahn, S.; Uhlig, F.; Thar, J.; Spickermann, C.; Kirchner, B. *Angew. Chem. Int. Ed.* **2008,** *47,* 3639–3641.

[7] Hunt, P. A.; Kirchner, B.; Welton, T. *Chem.-Eur. J.* **2006,** *12,* 6762–6775.

[8] Lehmann, S. B.; Roatsch, M.; Schöppke, M.; Kirchner, B. *Phys. Chem. Chem. Phys.* **2010,** *12,* 7473–7486.

[9] Elfgen, R.; Hollóczki, O.; Kirchner, B. *Acc. Chem. Res.* **2017,** *50,* 2949–2957.

[10] Anderson, J. L.; Armstrong, D. W. *Anal. Chem.* **2003,** *75,* 4851–4858.

[11] Baranyai, K. J.; Deacon, G. B.; MacFarlane, D. R.; Pringle, J. M.; Scott, J. L. *Austr. J. Chem.* **2004,** *57,* 145–147.

[12] Cassity, C. G.; Mirjafari, A.; Mobarrez, N.; Strickland, K. J.; O'Brien, R. A.; Davis, J. H. *Chem. Commun.* **2013,** *49,* 7590–7592.

[13] Kosmulski, M.; Gustafsson, J.; Rosenholm, J. B. *Thermochim. Acta* **2004,** *412,* 47–53.

[14] Hallett, J. P.; Liotta, C. L.; Ranieri, G.; Welton, T. *J. Org. Chem.* **2009,** *74,* 1864–1868.

[15] Boros, E. *et al. Chem. Commun.* **2010,** *46,* 716–718.

[16] *BASIL Process, BASF SE, World Patent WO2005/061416.* .

[17] Amigues, E. J.; Hardacre, C.; Keane, G.; Migaud, M. E.; Norman, S. E.; Pitner, W. R. *Green Chem.* **2009,** *11,* 1391–1396.

[18] Amigues, E.; Hardacre, C.; Keane, G.; Migaud, M.; Norman, S.; Pitner, W. *ECS Trans.* **2010,** *33,* 63–72.

[19] Amigues, E.; Hardacre, C.; Keane, G.; Migaud, M.; O'Neill, M. *Chem. Commun.* **2006,** 72–74.

[20] Wolff, A.; Pallmann, J.; Brunner, E.; Doert, T.; Ruck, M. *Z. Anorg. Allg. Chem.* **2017,** *643,* 20–24.

[21] Estager, J.; Holbrey, J.; Swadźba-Kwaśny, M. *Chem. Soc. Rev.* **2014,** *43,* 847–886.

[22] Brown, L. C.; Hogg, J. M.; Swadźba-Kwaśny, M. *Top. Curr. Chem.* **2017,** *375,* 78.

[23] Fumino, K.; Peppel, T.; Geppert-Rybczyńska, M.; Zaitsau, D. H.; Lehmann, J. K.; Verevkin, S. P.; Köckerling, M.; Ludwig, R. *Phys. Chem. Chem. Phys.* **2011,** *13,* 14064–14075.

[24] Cremer, T. *et al. Chem.-Eur. J.* **2010,** *16,* 9018–9033.

[25] Wulf, A.; Fumino, K.; Ludwig, R. *Angew. Chem. Int. Ed.* **2010,** *49,* 449–453.

[26] Hollóczki, O.; Gerhard, D.; Massone, K.; Szarvas, L.; Németh, B.; Veszprémi, T.; Nyulászi, L. *New J. Chem.* **2010,** *34,* 3004–3009.

[27] Rodríguez, H.; Gurau, G.; Holbrey, J. D.; Rogers, R. D. *Chem. Commun.* **2011,** *47,* 3222–3224.

[28] Hollóczki, O. *Inorg. Chem.* **2013,** *53,* 835–846.

[29] Wellens, S.; Brooks, N. R.; Thijs, B.; Van Meervelt, L.; Binnemans, K. *Dalton Trans.* **2014,** *43,* 3443–3452.

[30] Dillon, K.; Platt, A.; Schmidpeter, A.; Zwaschka, F.; Sheldrick, W. *Z. Anorg. Allg. Chem.* **1982,** *488,* 7–26.

[31] Wilkes, J. S.; Levisky, J. A.; Wilson, R. A.; Hussey, C. L. *Inorg. Chem.* **1982,** *21,* 1263–1264.

[32] Noda, A.; Hayamizu, K.; Watanabe, M. *J. Phys. Chem. B* **2001,** *105,* 4603–4610.

[33] Kirchner, B.; Seitsonen, A. P. *Inorg. Chem.* **2007,** *46,* 2751–2754.

[34] Schäfers, F. *JLSRF* **2016,** *2,* 96.

[35] Neese, F. *WIREs: Comput. Mol. Sci.* **2012,** *2,* 73–78.

[36] Becke, A. D. *J. Chem. Phys.* **1993,** *98,* 5648–5652.

[37] Lee, C.; Yang, W.; Parr, R. G. *Phys. Rev. B* **1988,** *37,* 785.

[38] Miehlich, B.; Savin, A.; Stoll, H.; Preuss, H. *Chem. Phys. Lett.* **1989,** *157,* 200–206.

[39] Grimme, S.; Antony, J.; Ehrlich, S.; Krieg, H. *J. Chem. Phys.* **2010,** *132,* 154104.

[40] Grimme, S.; Ehrlich, S.; Goerigk, L. *J. Comput. Chem.* **2011,** *32,* 1456–1465.

[41] Weigend, F.; Ahlrichs, R. *Phys. Chem. Chem. Phys.* **2005,** *7,* 3297–3305.

[42] Lu, T.; Chen, F. *J. Comput. Chem.* **2012,** *33,* 580–592.

[43] Ehrhardt, C.; Ahlrichs, R. *Theor. Chim. Acta* **1985,** *68,* 231–245.

[44] Treutler, O.; Ahlrichs, R. *J. Chem. Phys.* **1995,** *102,* 346–354.

[45] Weigend, F. *Phys. Chem. Chem. Phys.* **2002,** *4,* 4285–4291.

[46] Ahlrichs, R.; Bär, M.; Häser, M.; Horn, H.; Kölmel, C. *Chem. Phys. Lett.* **1989,** *162,* 165–169.

[47] VandeVondele, J.; Krack, M.; Mohamed, F.; Parrinello, M.; Chassaing, T.; Hutter, J. *Comp. Phys. Commun.* **2005,** *167,* 103–128.

[48] Becke, A. D. *Phys. Rev. A* **1988,** *38,* 3098.

[49] VandeVondele, J.; Hutter, J. *J. Chem. Phys.* **2007,** *127,* 114105.

[50] Goedecker, S.; Teter, M.; Hutter, J. *Phys. Rev. B* **1996,** *54,* 1703.

[51] Hartwigsen, C.; Gœdecker, S.; Hutter, J. *Phys. Rev. B* **1998,** *58,* 3641.

[52] Krack, M. *Theor. Chem. Acc.* **2005,** *114,* 145–152.

[53] Martinez, L.; Andrade, R.; Birgin, E. G.; Martinez, J. M. *J. Comp. Chem.* **2009,** *30,* 2157–2164.

[54] Brehm, M.; Kirchner, B. *J. Cheminfo.* **2012,** *4,* F1.

[55] Nyquist, R. A. *Appl. Spectr.* **1987,** *41,* 272–279.

[56] Pimentel, G. C. *J. Chem. Phys.* **1951,** *19,* 446–448.

[57] Berry, R. S. *J. Chem. Phys.* **1960,** *32,* 933–938.

[58] Burcat, A. *Combust. Flame* **2017,** *182,* 238–247.

[59] Fannin Jr, A. A.; Floreani, D. A.; King, L. A.; Landers, J. S.; Piersma, B. J.; Stech, D. J.; Vaughn, R. L.; Wilkes, J. S.; Williams, J. L. *J. Phys. Chem.* **1984,** *88,* 2614–2621.

[60] Sanders, J. R.; Ward, E. H.; Hussey, C. L. *J. Electrochem. Soc.* **1986,** *133,* 325–330.

[61] Weber, H.; Hollóczki, O.; Pensado, A. S.; Kirchner, B. *J. Chem. Phys.* **2013,** *139,* 084502.

[62] Shukla, M.; Srivastava, N.; Saha, S. *J. Mol. Struct.* **2010,** *975,* 349–356.